Published in final edited form as:
Anat Rec (Hoboken). 2014 April ; 297(4): 731–748. doi:10.1002/ar.22881.

CONTRASTING HISTOPATHOLOGY AND CRYSTAL DEPOSITS IN KIDNEYS OF IDIOPATHIC STONE FORMERS WHO PRODUCE HYDROXY APATITE, BRUSHITE, OR CALCIUM OXALATE STONES

Andrew P Evan[1,2], **James E Lingeman**[2], **Elaine M Worcester**[3], **Andre J Sommer**[4], **Carrie L Phillips**[5], **James C Williams**[1], and **Fredric L Coe**[3]

[1]Department of Anatomy and Cell Biology, Indiana University School of Medicine, Indianapolis, IN

[2]International Kidney Stone Institute, Methodist Hospital, Indianapolis, IN

[3]Nephrology Section, University of Chicago, Chicago, IL

[4]Department of Chemistry and Biochemistry, Miami University, Oxford, OH

[5]Department of Pathology, Indiana University Health, Indianapolis, IN

Abstract

Our previous work has shown that stone formers who form calcium phosphate (CaP) stones that contain any brushite (BRSF) have a distinctive renal histopathology and surgical anatomy when compared to idiopathic calcium oxalate stone formers (ICSF). Here we report on another group of idiopathic CaP stone formers, those forming stone containing primarily hydroxyapatite, in order to clarify in what ways their pathology differs from BRSF and ICSF. Eleven hydroxyapatite stone formers (HASF) (2 males, 9 females) were studied using intra-operative digital photography and biopsy of papillary and cortical regions to measure tissue changes associated with stone formation. Our main finding is that HASF and BRSF differ significantly from each other and that both differ greatly from ICSF. Both BRSF and ICSF patients have significant levels of Randall's plaque compared to HASF. Intra-tubular deposit number is greater in HASF than BRSF and non-existent in ICSF while deposit size is smaller in HASF than BRSF. Cortical pathology is distinctly greater in BRSF than HASF. Four attached stones were observed in HASF, three in 25 BRSF and 5–10 per ICSF patient. HASF and BRSF differ clinically in that both have higher average urine pH, supersaturation of CaP, and calcium excretion than ICSF. Our work suggests that HASF and BRSF are two distinct and separate diseases and both differ greatly from ICSF.

INTRODUCTION

Patients who form calcium stones in the absence of systemic disease, idiopathic calcium stone formers, are often lumped together clinically and even in research studies (Pak et al., 1980; Laerum and Larsen, 1984). But on careful inspection they are exceedingly

Corresponding Author: Andrew P. Evan, PhD, Department of Anatomy & Cell Biology, Indiana University School of Medicine, 635 Barnhill Drive, MS 5055, Indianapolis, IN 46220, aevan@iupui.edu, FAX: 317-278-2040.

heterogeneous in their renal histopathological pictures. A large fraction form stones predominantly composed of calcium oxalate (CaOx) (Coe et al., 2005); these patients, idiopathic CaOx stone formers (ICSF), form their stones on the surfaces of the renal papillae over interstitial deposits of apatite crystals (Randall's Plaque, RP) and the papillae, apart from the stones and plaque, are pristine (Evan et al., 2006b). The other great division form calcium phosphate (CaP) stones, and it is to them, idiopathic CaP stone formers (IPSF) the present paper turns its attention.

We have shown that patients who form stones that contain any brushite (BR, calcium mono-hydrogen phosphate) have a distinctive renal histopathology (Evan et al., 2005). Scattered ducts of Bellini (BD) and inner medullary collecting ducts (IMCD) are plugged with apatite crystals. These plugged ducts can be dilated massively, up to 20 times normal diameter; epithelial cells show extensive injury and loss, and involved ducts are surrounded by interstitial fibrosis. Although some papillae can be spared, the majority has at least a few plugged ducts, gross retraction, and dilated BD openings when visualized at the time of stone surgery. RP is present, but overgrowth of CaOx stones on plaque, which is the rule in ICSF (Miller et al., 2009), is very uncommon and overgrowth of CaP stones on RP has not been observed. Intra-tubular deposits, which appear yellow tinged beneath the urothelium (yellow plaque), often protrude out of the openings of dilated BD and it has been proposed but not as yet demonstrated that stones form on these exposed tubule plugs. Although the presence of BR in stones defines this group of patients, their stones may contain CaOx, CaP in the form of hydroxyapatite (HA), or both.

The other group of IPSF produce no BR phase but form stones containing HA variably admixed with CaOx (Parks et al., 2004). Here, we focus on hydroxyapatite stone formers (HASF) without systemic disease and attempt to clarify in what ways their pathology differ from BR stone formers (BRSF) and ICSF. We have used a simple cut point and despite so arbitrary a criterion find extreme differences in the renal tissues: ICSF never form BD or IMCD deposits whereas HASF always do. Likewise, HASF and BRSF differ in the particulars of their renal pathology and crystal deposits. These differences seem sufficient to establish ICSF, BRSF, and HASF as three distinct and separable clinical phenotypes.

METHODS

Subjects

Our subjects were defined by the type of stones they formed, as we have described previously (Parks et. al., 2004), using conventional stone analyses from commercial laboratories. We calculated the average percent of CaP in all analyzed stones from each patient as a fraction of total stone mineral. We defined as HASF those with stone composition of >50% CaP, and no BR in any stone, We defined as BRSF those with BR in any stone. No patient had systemic disease as a cause of stones. Specifically we excluded renal tubular acidosis by requiring normal serum bicarbonate and potassium levels. These patients represent all patients with HA and BR stones who underwent papillary and cortical biopsy at the time of stone surgery since the inception of the biopsy protocol in 1999.

We studied 11 HASF patients (Tables 1–3, cases 1–11) in whom, with one exception, no stones contained BR. This exception (Table 2, patient 5) formed a stone from one kidney with 100% BR, but we biopsied the other kidney from which all stones were HA; the average stone composition of all stones from this patient was 55% HA. In addition, we studied 15 BRSF (Tables 1–3, cases 12–26) who formed stones that contained BR with a wide and variable admixture of CaOx and HA. We have detailed the metabolic data and histopathology of another 10 BRSF in an earlier publication (Evan et. al., 2005); we include some previously unreported data for these 10 patients here. We also include previously unreported data for 30 ICSF who have been the subject of earlier publications (Evan et. al., 2003; Evan et. al., 2008a).

Clinical laboratory studies

Two twenty-four hour urine samples were collected in these patients while they were eating their free choice diet and off medications including potassium citrate. In urine we measured volume, pH, calcium, oxalate, citrate, phosphate, uric acid, sodium, potassium, magnesium, sulfate and ammonia and calculated supersaturation (SS) with respect to CaOx, BR and uric acid using methods detailed elsewhere. Routine clinical blood measurements were made on bloods drawn for clinical purposes (Table 2).

Biopsy protocol and plaque area determination

During percutaneous nephrolithotomy (PNL) all papillae in each patient were digitally imaged as described elsewhere for determination of white and yellow plaque area (Evan et al., 2006b; Coe et al., 2010). The surgeon determined papillary anatomy as normal, eroded and/or flattened; we assigned 0 to normal and 1 to eroded or flattened and calculated an injury score as the sum divided by the number of papillae evaluated. He also evaluated calyceal dilation as normal, mild, moderate or severe. We assigned corresponding values of 0, 0.5, 1, and 2 and calculated a dilation score as the sum divided by the number of papillae.

Papillary biopsies were taken from all HASF and BRSF patients and consisted of a biopsy of the upper pole, inter-polar and lower pole papillum and one from the cortex in 22 of the 26 cases (Excluding cases 10, 22, and 26). No biopsy site inspected intra operatively displayed significant hemorrhage and no post-operative complications related to the biopsy procedures occurred in any patient. The study was approved by the Institutional Review Board Committee for Clarian Health Partners (#98-073).

Tissue analysis

General—Twenty-six papillary and twenty-two cortical biopsies were studied using light microscopy. All biopsy (cortical and papillary) specimens were immersed in 5% paraformaldehyde in 0.1 mol/L phosphate buffer (PPB) (pH 7.4). In addition we use here unpublished cortical data from 30 ICSF (Evan et al., 2008a).

Light microscopy—Papillary and cortical biopsies were dehydrated through a series of graded ethanol concentrations to 100% ethanol prior to embedment in a 50/50 mixture of Paraplast Xtra (Fisher) and Peel-away Micro-Cut (Polysciences). Papillary biopsies fixed in 100% ethanol were directly embedded in a 50/50 mixture of Paraplast Xtra (Fisher) and

Peel-away Micro-Cut (Polysciences). Twelve serial sections were cut at 4μ and stained with the Yasue metal substitution method for calcium histochemistry (Yasue, 1969), Tamm-Horsfall protein (THP) for immuno localization, Hematoxalin & Eosin for routine histological examination or Jones' silver stain for the semi-quantitation of glomerulosclerosis and the Masson Trichrome stain to determine sites of interstitial fibrosis at the light microscopic level. An additional set of serial sections was cut at 7μ for infrared analysis. The immunohistochemical slides were deparaffinized and rehydrated through graded alcohols and blocked for nonspecific protein binding to the second antibody using 10% normal serum in 0.1 mol/L phosphate-buffered saline (PBS) plus 10 mM ammonium chloride ad 3% Blotto, at room temperature for 1 hour. The THP sheep anti-human polyclonal antibody (Chemicon, Tenecula, CA) was used at a 1:50 dilution. The secondary antibody was rabbit anti-sheep fluorescein (Jackson ImmunoResearch, West Groove, PA) diluted 1:150 in 2% normal rabbit serum/PBS. The secondary antibody was incubated on the slides at room temperature for 1 hour. The slides were then rinsed three times in PBS, once in double distilled water, cover-slipped with Vectashield mounting medium for fluorescence with 4′,6-diamidine-2-phenylidole-dihydrochloride (DAPI, Vector Laboratories, Burlingame, CA), sealed with clear nail polish and immediately studied.

A renal pathologist blinded to the patient information performed a semi-quantitative analysis (Evan et al., 2005) using the Jones' silver stained cortical sections from all patients. We included all available measurements from 10 of our 11 HASF, 12 of our 15 BRSF newly described here, previously unpublished data from 9 of our prior 10 BRSF, and all of our prior 30 ICSF.

Tubular atrophy and interstitial fibrosis were independently scored on a scale of 0 to 3 (0 = none, 1 = mild or <34% of sample, 2 = moderate or 34–66%, and 3 = severe or >66%). Glomerulosclerosis was defined as increased mesangial matrix with or without wrinkling, thickening and/or collapse of glomerular basement membranes. Sclerosis of individual glomeruli was scored as segmental (<25% = mild; 25 to 75% = moderate) or global (>75% = severe or total obsolescence). The total number of glomeruli observed and the number of glomeruli in each of the three categories of sclerosis were recorded. We calculated a glomerular injury score as the sum of glomeruli with segmental sclerosis + 2* those with moderate sclerosis + 4* those with global sclerosis divided by the number of glomeruli scored. To get as high as 2 required all have moderate sclerosis or those with mild or no sclerosis be balanced with some globally sclerosed.

Transmission electron microscopy (TEM). TEM was performed as described previously from this laboratory (Evan et al 2008b).

Infrared—Attenuated Total Internal Reflection (ATR) Fourier Transform Infrared Microspectroscopy (μ-FTIR) was used as described elsewhere (Evan et al., 2005). Analyses were performed on sites of Novel interstitial plaque structures (NIPS), and intraluminal deposits in all HASF patients.

μCT—All papillary biopsies underwent μCT analysis with the SkyScan-1072 (Vluchtenburgstraat 3, B-2630 Aartselaar, Belgium) high-resolution desk-top μCT system

allowing nondestructive mapping of the location and size of the crystalline deposits within a biopsy specimen. This μCT system can generate a tissue window so that both the mineral deposit and tissue organization are seen at the same time. For this protocol, biopsies are quickly dipped in a 1:10 dilution of Hypaque (50%, Nycomed Inc., Princeton, NJ)/PBS, then coated with a thin layer of paraffin and mounted in the center of a small chuck which is then locked into place in the machine. The sample was positioned in the center of the beam, and the system configuration was set at 35 kV, 209 μA, 180° rotation, with flatfield correction. Images were saved to CD's and reconstructed with Cone-Reconstruction software by SkyScan. These images were then reconstructed into 3D images with SkyScan's CTAn + CTVol software. These images allowed us to properly orient each biopsy for future light microscopic analysis. The 3D software was used to generate quantitative measurements of deposit size (mm) and density (mm^3).

A second μCT system, the Scanco μCT 20 instrument (Scanco Medical AG, Basserdorf, Switzerland) was used to determine mineral composition of the crystalline deposits in papillary biopsies analyzed by the SkyScan μCT device. This system does not generate a tissue window. We used our recently published method (Evan et al., 2008b) to determine the μCT attenuation value for each crystalline deposit to determine its mineral composition. The attenuation value for cystine has a range between 8,500 and 10,000, HA is 21,000 to 22,000, and CaOx and BR are at 17,000 to 20,000. The system utilized a 7-μm spot-size microfocus x-ray source (0.16 mA, 50 kVp) that was detected by a charge coupled device array with 1024 elements. The scans on each specimen were completed using standard resolution (512 × 512 pixels) and a 17.4 mm specimen holder, which produced image slice thicknesses and pixel widths of 34 μm.

Stone analysis

Seven of the 11 HASF had their stones analyzed by a single lab (Beck Laboratories, Indianapolis IN) using IR + polarization microscopy. All of these 7 were re-analyzed by one of us (JW) using IR. Unlike common stone analysis we used all of each stone for IR, not a small sample. In none could we find any trace of BR except for patient 5. The other 4 cases had stones analyzed by outside commercial laboratories. Stones for the BRSF and ICSF were likewise analyzed by Beck as well as outside commercial laboratories.

Statistical Analysis

We compared ICSF, BRSF and HASF using ANOVA concerning all 24-hour urine values. We considered six papillary disease markers: deposit numbers, deposit size, papillary injury, calyceal dilation, yellow plaque and RP areas. We compared BRSF to HASF for each using t-tests. We sought all possible correlations between markers within groups, and between markers and urine stone risk measurements using simple correlation. We compared slope dependencies using general linear models with appropriate cross products.

RESULTS

Patients

We studied 11 HASF (Tables 1–3**, cases 1–11)** and 15 new BRSF (Tables 1–3**, cases 12–26**). Urine stone risk factors (Table 3) showed the variable idiopathic hypercalciuria (urine calcium >300 mg/day), and hypocitraturia (urine citrate <450 mg/day) that we and others have previously described in ICSF and IPSF (Parks et al., 2004; Gault et al., 1991).

Intra-operative Images

We observed tubule plugging in all of the 11 HASF. Dilated BD were evident (Figure 1**, panels a and b**); a deposit is seen protruding from one of these (Figure 1**, panels a and b, at asterisk).** Intra-tubular, sub-urothelial deposits (yellow plaque) (Figure 1**, panels c – f, arrows**) were moderately abundant in 8 patients (**panels c and d**) and very abundant in the other three (**panels e and f**); virtually all papillae contained some deposits. RP was very abundant in one patient but scanty in the others (Figure 1**, panels b and d, respectively**). Papillary architecture was abnormal in all HASF except patient 9 (not shown); two patients, 3 and 5 (Figure 1**, panels e and f),** showed severe retraction. Operative findings in the BRSF were similar to those we have already documented (Figure 2 a – f).

Stones and crystal deposits

Stones growing on plugs—Using micro-CT analysis (Figure 3**, panels a and b, BRSF patient 22 in tables)**, a stone overgrowth on a tubule plug in a BRSF was composed of BR with a thin surface layer of CaOx whereas the stalk - the original tubule plug - contained HA, BR, and CaOx. Another stone, from HASF patient 8, also formed on a BD plug (Figure 3**, panels c and d**); the body of the stone and the plug are HA; the stone surface had traces of CaOx. Findings in these two patients are the same as in the other patients.

Stones growing on plaque—Among ICSF (Table 4) an average of 10 stones per patient have been found growing on RP. Among BRSF we found 3 stones on RP among 25 patients (Table 4). Among HASF we found 2 CaOx stones and 4 HA stones among 11 patients. Overall the rates of stone growth on RP among ICSF exceeded that of CaP stone formers by about 100 fold.

RP and novel interstitial plaque structures (NIPS)—Only three of the 11 HASF (Table 1**, patients 1, 6, 9,**) exhibited above normal (0.5% – 1%) abundance of RP [9] (Figure 4**, panel a, arrowheads, patient 6**), whereas almost all BRSF did so. As always (Evan et al, 2003) RP consisted of layers of HA micro-spherules and organic matrix alternating in a lamellar pattern (Figure 4**, panel a, insert**). By contrast, five HASF (Table 1**, patients 1 – 5**) displayed varying amounts of a newly described type of interstitial calcification that we term NIPS. In regions of sparse or moderate NIPS involvement (Figure 4**, panels b and c, arrows**), NIPS were irregular randomly distributed laminar deposits of interstitial HA and matrix. Micro-spherules were few in number and lack the multiple alternating laminae of crystal and matrix invariably found in RP. Instead, each NIPS was a crystal deposit surrounded by a single thin layer of matrix (Figure 4**, panel b, insert**). NIPS were not associated with basement membranes, any particular tubular segment, or cell debris

whereas RP forms in the basement membranes of the thin loops of Henle (Evan et al., 2003) (Figure 4**, compare panel a to panels b–d**). NIPS have not been found thus far in ICSF or BRSF.

At higher magnification, NIPS were plate - like shapes around the lumens of capillaries or loops of Henle (Figure 4, **panel d**). Like RP, NIPS did not expand or distort the interstitial space; they simply filled it as if producing a crystal - matrix cast. In regions that contained extensive amounts of NIPS (Figure 5**, panels a and b)**, large islands of crystal resided within so sparse a matrix that the appearance was mainly of crystal. This was the exact opposite of the crystal - matrix ratio found in RP (Figure 5**, panel c)**. Using TEM the larger ratio of crystal to matrix in NIPS vs. RP was clearly evident (Figure 6**, compare panels a and b to panels c and d**).

Extensive fibrosis surrounded large NIPS deposits (Figure 5**, panel a**), whereas even large accumulations of RP, and smaller amounts of NIPS, did not evoke an inflammatory reaction (Figure 5**, panel c**). However, the large NIPS deposits resided near tubules plugged with HA, and such plugging can, itself, evoke an inflammatory reaction (Coe et al., 2010), so the role of NIPS vs. tubule plugging to evoke inflammation and fibrosis cannot be resolved with our available tissue.

One possible source of the NIPS crystal is exotubulosis (Vervaet et al., 2009) from plugs in IMCD or BD into the papillary interstitium. Another is formation within the interstitium driven by local CaP saturation. In the first case, crystals would be in contact with tubule fluid distal to the thick ascending limbs and therefore carry Tamm-Horsfall protein (THP), a molecule known to adsorb strongly to HA (Thurgood and Ryall, 2010). In the second, THP would not have access to the crystals because the interstitium does not normally contain THP (Peach et al., 1988). To distinguish these alternatives we stained NIPS with anti-THP antibody; no staining of NIPS was found (Figure 5**, panel d**) even though adjacent tubule lumens stained as expected.

Quantitative Contrast of HASF and BRSF

Size and numbers of tubule deposits, and RP—Among our 25 BRSF, average tubule deposit size ranged from 0.5 to 3 mm (Figure 7**, left panel, closed circles, y axis)** and numbers of deposits ranged from 1 to 10 per mm^3 (Figure 7**, left panel, x axis**). RP abundance (Figure 7**, right panel, x axis, filled circles**) ranged from 2 to 8% of papillary surface; our normal range is 0.5% to 1% and ICSF average 7% (Coe et al., 2010). HASF (**triangles**) formed smaller deposits (Figure 7**, both panels, y-axis**) than BRSF (**circles**) (0.41±0.28 vs. 1.59±0.81, HASF vs. BRSF, respectively, $p<0.001$; means in mm ± SD). Ranges of deposit density (**x axis left panel**) overlapped (12±15 vs. 4±2, HASF vs. BRSF, respectively, p NS; means are #/mm^3). Three HASF (Figure 7**, left panel**) had extremely high numbers of deposits. We omit ICSF who have only plaque. Presence of NIPS **(black triangles**) did not associate with specific values of RP, or deposit size or number.

Deposit size correlated with deposit number in BRSF ($r=0.44$, $p=0.04$). In the same analysis in HASF, $r=0.46$, but p=NS perhaps because of the smaller sample size (11 vs. 25). Nevertheless, the slope dependence of deposit size on deposit number differed between the

two groups. In a general linear model that included BRSF and HASF combined, with deposit size as dependent, deposit number was a significant covariate (F=6.2, p=0.019) and the cross product of patient type by deposit number was significant. There was no relationship between deposit size and RP area in either group, and RP abundance (%) in HASF was lower than in BRSF (1.3±2.4 vs. 3.5±2.5, p=0.02, HASF vs. BRSF, respectively) (Figure 7**, right panel**).

Yellow plaque—The fraction of papillary surface (%) covered by yellow plaque **(METHODS)** correlated with the number of deposits as measured in tissue by micro-CT (Figure 8**, left panel)** in HASF (r=0.98, p<0.001) but not in BRSF (r=0.12, p, NS). This suggests that in HASF the amount of yellow plaque seen at surgery is a practical gauge of deposit number in papillary tissue. Yellow plaque abundance of HASF exceeded BRSF (7.2 ±10 vs. 1.7 ±1 (area %)); the difference was not quite significant using separate variance t tests (p=0.09), but was significant with pooled variances (p = 0.02). The range of yellow plaque abundance was smaller for BRSF than HASF and the non-parametric ellipse of containment for BRSF falls within that of HASF (Figure 8**, left panel).** Yellow plaque area appears to vary with deposit size in HASF but not BRSF (Figure 8**, right panel).**

Dilation and Injury—During surgery, papillary injury was noted as present or absent and calyceal dilation graded from absent to severe for each papillum. We created a unitless score for each **(METHOD**S). In HASF, dilation (Figure 9) was greater than in BRSF or ICSF (0.79±0.1 vs. 0.17±0.1 vs. 0.22±0.1, HASF vs. BRSF vs. ICSF, respectively; p<0.01 for HASF vs. ICSF or BRSF) and dilation correlated with injury (HASF, r=0.75 p=0.013; ICSF or BRSF r<0.001, p, NS). In BRSF, dilation correlated with deposit size (r=0.49, p=0.02); this was not true in HASF or ICSF. Injury was greater in HASF vs. ICSF (0.37± 0.1 vs. 0.53± 0.1, p=0.007). Differences were not significant between BRSF and HASF or between BRSF and ICSF. Overall BRSF and HASF differed with regard to calyceal dilation but not injury. Values are means with SEM.

Cortical histopathology—We had cortex from 10 of our 11 HASF, 21 of our 25 BRSF (9 from our prior series and 12 from the current series), and all 30 ICSF. BRSF (Figure 10**, left panel**) frequently had tubular atrophy or interstitial fibrosis whereas this occurred uncommonly in HASF and ICSF (Figure 10**, left panel, black triangles**). The proportions for interstitial fibrosis are unlikely by chance (X^2= 16.6, p=0.01) but not those for tubular atrophy (X^2 = 8.5, p=0.2). Values below 1 are omitted from the left panel of the figure for visual clarity but included in the proportion calculations.

Glomerular injury was scored conventionally and from the scores we made a continuous variable reflecting severity and numbers of involved glomeruli (**METHODS**). A combined score using glomerular injury and the higher of either tubule atrophy or interstitial fibrosis (Figure 10**, right panel)** identifies 3 patients (2 HASF, 1 BRSF) with elevated glomerular injury scores but no more than 1+ tubulo-interstitial changes (Table 2 **details findings in each HASF and the current 15 BRSF**), 4 patients with glomerular and tubulo-interstitial disease (1 HASF, 3 BRSF), and 11 patients with mainly tubulo-interstitial disease (1 HASF, 8 BRSF, 2 ICSF). Out of 30 cases, only 2 ICSF had interstitial changes above a score of 1,

and none had significant glomerular disease with a glomerular score above 1, while 4/11 HASF and 12/25 BRSF had significant cortical injury. Figure 11a–c show the range of interstitial, tubular and glomerular changes seen by light microscopy in the HASF and BRSF patients.

Clinical Laboratory Measurements—We had 24 hour urine data for 8/11 HASF, 19/25 BRSF, and 27/30 ICSF (Table 3 **shows HASF and current 15 BRSF**). Using ANOVA, with urine creatinine (mg/d) as a covariate (except for pH), we found significant differences between BRSF and ICSF: volume (L/d; 2±0.13 vs. 1.54±0.12), calcium (mg/d; 348±28 vs. 237±54), magnesium (mg/d; 128±7 vs. 106±6), pH (6.23±0.1 vs. 5.87±0.08), and SS CaP (2.1±0.2 vs. 1.2±0.1), $p<0.01$ all comparisons. All 24-hour urine values in HASF were similar to those in BRSF but values in HASF did not differ from ICSF at a statistically significant level perhaps because of the small HASF group size. Urine data for ICSF are not shown in the table because values from the original report of 15 cases have been published. We present here the overall mean for all 30 cases (15 published + 15 new) because the data are not available anywhere else, and we have made comparisons using those combined data.

There were no correlations between any urine measurement and measurements of deposits, yellow plaque, injury, dilation, and cortical changes either considering all three groups together or within group except that number of deposits correlated with SS CaP for BRSF and HASF taken together ($r=0.64$, $p=0.045$). For BRSF and HASF taken together in a stepwise general linear model, RP area was proportional to urine calcium (standard coefficient = 0.49, $F=8$, $p<0.001$) but urine volume, pH, oxalate, phosphate, citrate, and ammonia did not enter the regression. RP area in the group of 15 ICSF for whom we have published the measurement has already been reported as proportional to urine calcium and inversely proportional to urine volume and pH (Kuo et al., 2003).

Obstruction and conversion from CaOx stones

Although we cannot be certain, it would appear possible that conversion of stone type occurred in HASF cases 3 and 11 (Table 2). Among the BRSF we have evidence favoring conversion of stone type in 5 patients (Table 2**, patients 12, 13, 18, 21, 25**) who had no BR in their first stone, which contained mainly CaOx. Conversion of stone type does not necessarily mean conversion from the ICSF phenotype in which stones grow over RP to the situation in BRSF and HASF in which RP overgrowth is rare. Composition changes could reflect differing urine SS conditions in patients who form their stones over plugs or in free solution. We make this remark because despite ample RP we found only rare stones growing on it in BRSF.

Among BRSF 7/15 had an obstructive lesion of the urinary tract, either congenital or acquired. This seems particularly notable in the female BRSF. Cases 18 and 21 had CaOx stones in one kidney and BR in the other; the side with BR showed chronic urinary tract obstruction. In case 19 the obstructed side had a staghorn composed almost entirely of CaOx mixed with HA, with a thin coating of BR; the stone from the opposite side also contained BR. Among the HASF, the majority of whom were women, obstructive disorders were not prominent even though calyceal dilation was.

μFTIR

In HASF, we performed μFTIR analysis of tubule deposits and regions containing NIPS (Figure 12). All sites of both contained only biological HA. We have reported μFTIR of deposits in 10 of the 25 BRSF previously (Evan et al., 2005), and did not perform μFTIR in the newly studied BRSF.

DISCUSSION

Our main finding is that HASF and BRSF differ in their tissue expression of disease and both differ from ICSF. HASF produce smaller deposits than BRSF, but deposits are more numerous and widespread so most papillae show some damage from them. BRSF form fewer but larger deposits that damage some papillae to a greater degree than is usual in HASF but leave many papillae normal. RP abundance in BRSF is in the range of ICSF but thus far we have found only 3 CaOx stones growing on RP in 25 BRSF whereas typical ICSF have 5–10 stones on RP per patient - a hundred fold difference. RP abundance in HASF is less than ⅓ that of BRSF; however, 2 CaOx and 4 apatite stones were found growing on RP of 4 of the 11 HASF patients. NIPS are common in HASF, and not present in BRSF. HASF have an obvious female preponderance not present in ICSF or BRSF. Perhaps of greatest clinical importance, cortical pathology is distinctly greater in BRSF than HASF and far greater than in ICSF. The differing patterns of deposits, papillary injury, RP abundance, production of NIPS, and cortical injury suggest that BRSF and HASF are not simply variations of a single disease but rather two distinct and separate diseases, and both differ from ICSF, which also seems a distinct disease in itself.

BRSF and HASF differ from ICSF in their clinical physiology in that compared to ICSF both have higher average urine pH, SS CaP and calcium excretion (Table 4). We presume the higher CaP content of stones in BRSF and HASF vs. ICSF reflects the higher pH and SS CaP as we found strong association between % CaP in stones and both urine pH and SS CaP in our much larger series of stone formers. We presume tubule plugging is absent in ICSF because of their lower SS CaP. The higher SS CaP is mainly due to higher urine pH but why urine pH is higher is unknown and our present data do not provide new clues to its pathogenesis.

We do not know why HASF and BRSF differ so widely from each other in patterns of tissue mineralization, as they do not differ from each other with respect to urine pH, calcium excretion and CaP SS. However we can perhaps propose a new working hypothesis that can explain three of the differences highlighted in Table 4 by bolding. BR is the earliest and most soluble CaP phase that forms in urine (Pak et al., 1971; Qiu and Omer, 2008), and our calculations of CaP SS should more properly be called BR SS. BR fosters nucleation of CaOx and HA that both can cannibalize BR by taking up its calcium atoms (Tang et al., 2006). Therefore, though kinetically favored as a starting phase, BR will have a low abundance in tubule fluid and urine compared to CaOx and HA. Assume, however, that tubule fluid and urine of BRSF can inhibit nucleation of HA more strongly than ICSF or HASF. If this were true then BR abundance would increase allowing formation of BR stones admixed variably with CaOx. Fewer tubules would be plugged with HA in BRSF than HASF despite equal CaP SS. Inhibition of HA nucleation would inhibit CaOx overgrowth

on RP, which requires that HA nucleate over RP that has been exposed to urine by loss of urothelial integrity,

In studies of men and women, there is experimental evidence that nucleation inhibition can vary among subjects (Asplin et al., 1991; Asplin et al., 2002). For example, the upper limit of metastability (ULM) – the SS at which BR nucleation occurs in urine – is marginally higher in normal vs. calcium stone formers and the BR SS marginally lower. Therefore, the distance between SS and ULM, which is the crucial determinant of nucleation, is larger in normal subjects than in stone formers. We propose by homology that BRSF have a higher ULM for HA nucleation than HASF or ICSF so BR can accumulate instead of converting to HA. A key prediction of our hypothesis is that urine from BRSF will inhibit BR to HA conversion in vitro, a feasible experiment beyond the scope of the present paper.

Our one assumption could explain a number of the differences between BRSF, ICSF and HASF. ICSF and BRSF both have abundant RP (Kuo et al., 2003). In ICSF HA forms in a matrix of urine molecules that cover the surface of RP exposed to urine via loss of urothelial integrity (Evan et al., 2008a). CaOx stones grow over the HA. If HA nucleation were blocked in BRSF, CaOx overgrowth on RP would be substantially reduced and BR remain an abundant urine phase that could form stones in free solution. Because BR promotes CaOx nucleation (Tang et al., 2006), stones can be admixed. Minor amounts of HA may be found in stones. This idea predicts what we already know: BRSF have abundant plaque but rarely form stones on it. Likewise stone composition could convert between BR and CaOx as variations of BR vs. CaOx SS from life style changes or treatment alter the relative stability of the two phases. CaOx stones would be presumed to form in free solution as they are very uncommon as RP overgrowths.

Even if HA crystallization is inhibited in BRSF, BR itself can be made rapidly and is abundant enough to form clinically relevant stones (Tang et al., 2006); why then are tubule plugs less numerous than in HASF and why are they HA not BR? We propose a second hypothesis: Tissue injury by ESWL, obstruction, and PNL impair local tubule acidification so that intra-tubular pH increases markedly and HA forms despite inhibitors because of its extreme insolubility at high pH (Parks et al., 2004). Any BR that had formed would be cannibalized by HA. The large size and focal distribution of plugs may reflect their formation in damaged tissue. In support of a role for injury, we have found that ESWL rates in BRSF exceed those of ICSF and HASF (Evan et al., 2005; Parks et al., 2009). Likewise, injury may account for the greater cortical fibrosis and tubule atrophy in BRSF. In the present series Table 1 shows higher amounts of ESWL in our BRSF than in the HASF which supports this speculation.

If we simply assume that HA inhibition is no greater in HASF than in ICSF, the higher CaP SS will drive nucleation of BR that will convert to HA and CaOx. Stones will be made of HA and CaOx. Given high BR SS, BR will form and promote HA that plugs BD and IMCD as occurs in RTA and with drugs like topiramate (Fukumoto et al., 2011) and acetazolamide (Barbey et al., 2004). The scanty RP of HASF is not explained, and remains an open issue. Because RP is scanty, stones will not form mainly as overgrowths as in ICSF but as overgrowths on plugs or in free solution. Urine citrate is certainly part of the system of

molecules that can inhibit HA nucleation, but we were unable to document convincing hypocitraturia in the HA patients. Likewise very high urine pH from citrate medications could raise urine pH and promote HA formation, but our treatment records are simply not refined enough to attempt to link such treatment to stone type.

NIPS have only been described anatomically in one prior paper in which the patients were labeled ‘stone formers’ with no further information (Burry et al., 1976). In contrast to RP, NIPS do not form in thin limb basement membranes as laminated micro-spherules of apatite and organic matrix. We believe, but cannot prove, they form in the interstitial compartment as tiny irregular crystal deposits that grow in situ; this is entirely unlike RP, which transforms via coalescence of micro-spherules to form a matrix pool containing islands of apatite crystals (Evan et al., 2003). By contrast, NIPS are large deposits of crystal surrounded by scanty borders of matrix material, a difference that may reflect a differing mode of formation. Unlike RP, NIPS do not migrate to the sub-urothelial space, and therefore are invisible to the surgeon. When large, NIPS evoke an inflammatory reaction that is not found around even the most extensive collections of RP (Evan et al., 2003); but in our present material we cannot exclude that the inflammation is arising from nearby tubules plugged with HA.

NIPS deposits are not dystrophic calcifications, which inevitably associate with remnants of tubular cells. We do not find such remnants, or atrophic tubules, within or surrounding NIPS deposits, even the largest ones within areas of considerable inflammation. Crystals from hypercalcemia typically deposit in tubule lumens in the outer medulla, not in the interstitium (Burry et al., 1976). Scarring from infection and reflux nephropathy do not have a pattern of interstitial calcification (Weiss et al., 2007).

We have reported calcifications that resemble NIPS in THP knockout mice (Liu et al., 2010). They are exclusive to the deep papillary interstitial space, and appear as collections of irregularly shaped crystal deposits with more matrix than NIPS but less than RP. Like NIPS they do not accumulate beneath the urothelium. They do not associate with loops of Henle as RP does, and they do not elicit an inflammatory reaction even when massive. These animals form copious crystals and often obstruct their ureters, so obstructive uropathy is frequent. Infection was not noted in these animals. We have also observed similar deposits in NHERF (NHE3 regulating factor) knockout mice with hypercalciuria (Evan et al., 2010b). As in the THP knockout, deposits were irregular and occurred in deep medullary interstitium unassociated with any nephron segment; but the amount of deposit was much less than in the THP knockout animals. Since two rather different kinds of animal models both produce NIPS - like deposits, some common elements of the models must be presumed to cause them, and could in principle be sought as a clue to the human form.

We offer here the first descriptions of human stones growing over BD plugs. In the BRSF the plug itself was an amalgam of HA, BR, and CaOx not so much mixed together as present in their own separate regions of the plug. This is not in disagreement with our pathogenetic hypothesis. If via injury an IMCD and BD lost their normal acidification regulation, CaP SS and pH would rise but some BR remain present because conversion from BR to HA is partially inhibited. The CaOx could arise simply from nucleation on injured cells or BR or

HA crystals. In patients with distal renal tubular acidosis we found both HA and CaOx in BD plugs (Evan et al., 2007). In the HASF the plug was pure HA which is what our hypothesis, preliminary as it is, would predict.

Whether due to injury from procedures or from the primary disease processes themselves, the cortical pathology of BRSF appears substantial (Evan et al., 2005). Levels of even moderate cortical interstitial fibrosis and tubule atrophy connote significant renal disease even in the absence of reduced glomerular filtration rate. Our protocols did not include urine protein measurements so we cannot correlate with level of albuminuria. We found no association between cortical changes and presence of diagnosed hypertension. The clinical meaning of cortical pathology in BRSF must await larger and longer studies. The present work suffices only to provide awareness that such pathology exists. However, others have shown (Gambaro et al, 2001; Keddis and Rule, 2013) that nephrolithiasis appears to increase risk of progression to renal failure, and perhaps our findings are an early stage of such a process.

Our work suggests that there are at least three different phenotypes with respect to patterns of tissue mineralization and injury that can be found among idiopathic calcium stone formers with IH, and stone type is the best clue to the pattern that exists in a given patient. At present the mechanisms that result in these differing patterns are unclear, and will require further studies to clarify

Acknowledgments

Grant sponsor: NIH; Grant number: PO1 DK56788

Reference List

Asplin JR, Parks JH, Chen MS, Lieske JC, Toback FG, Pillay SN, Nakagawa Y, Coe FL. Reduced crystallization inhibition by urine from men with nephrolithiasis. Kidney Int. 1999; 56:1505–1516. [PubMed: 10504502]

Asplin JR, Parks JH, Nakagawa Y, Coe FL. Reduced crystallization inhibition by urine from women with nephrolithiasis. Kidney Int. 2002; 61:1821–1829. [PubMed: 11967033]

Barbey F, Nseir G, Ferrier C, Burnier M, Daudon M. Carbonic anhydrase inhibitors and calcium phosphate stones. Nephrologie. 2004; 25:169–172. [PubMed: 15455790]

Burry AF, Axelsen RA, Trolove P, Saal JR. Calcification in the renal medulla: A classification based on a prospective study of 2261 necropies. Human Pathol. 1976; 7:435–449. [PubMed: 939540]

Coe FL, Evan A, Worcester E. Kidney stone disease. J Clin Invest. 2005; 115:2598–2608. [PubMed: 16200192]

Coe FL, Evan AP, Lingeman JE, Worcester EM. Plaque and deposits in nine human stone diseases. Urol Res. 2010; 38:239–247. [PubMed: 20625890]

Evan AP, Lingeman JE, Coe FL, Parks JH, Bledsoe SB, Shao Y, Sommer AJ, Patterson RF, Kuo RL, Grynpas M. Randall Plaque of patients with nephrolithisis begins in basement membranes of thin loops of Henle. J Clin Invest. 2003; 111:607–616. [PubMed: 12618515]

Evan AP, Lingeman JE, Coe FL, Shao Y, Parks JH, Bledsoe SB, Phillips CL, Bonsib S, Worcester EM, Sommer AJ, Kim SC, Tinmouth WW, Grynpas M. Crystal-associated nephropathy in patients with brushite nephrolithiasis. Kidney Int. 2005; 67:576–591. [PubMed: 15673305]

Evan AP, Coe FL, Lingeman JE, Shao Y, Matlaga BR, Kim SC, Bledsoe SB, Sommer AJ, Grynpas M, Philips CL, Worcester EM. Renal crystal deposits and histopathology in patients with cystine stones. Kidney Int. 2006a; 69:2227–2235. [PubMed: 16710357]

Evan A, Lingeman J, Coe FL, Worcester E. Randall's plaque: pathogenesis and role in calcium oxalate nephrolithiasis. Kidney Int. 2006b; 69:1313–1318. [PubMed: 16614720]

Evan AP, Lingeman J, Coe F, Shao Y, Miller N, Matlaga B, Phillips C, Sommer A, Worcester EM. Renal histopathology of stone-forming patients with distal renal tubular acidosis. Kidney Int. 2007; 71:795–801. [PubMed: 17264873]

Evan AP, Coe FL, Gillen D, Lingeman JE, Bledsoe S, Worcester EM. Renal intratubular crystals and hyaluronan staining occur in stone formers with bypass surgery but not with idiopathic calcium oxalate stones. Anat Rec. 2008a; 291:325–334.

Evan AP, Lingeman JE, Coe FL, Miller N, Bledsoe S, Sommer A, Williams J, Shao Y, Worcester E. Histopathology and surgical anatomy of patients with primary hyperparathyroidism and calcium phosphate stones. Kidney Int. 2008b; 74:223–229. [PubMed: 18449170]

Evan AP, Lingeman JE, Coe FL, Bledsoe SB, Sommer AJ, Williams JC Jr, Krambeck AE, Worcester EM. Intra-tubular deposits, urine and stone composition are divergent in patients with ileostomy. Kidney Int. 2009; 76:1081–1088. [PubMed: 19710630]

Evan AP, Lingeman JE, Worcester EM, Bledsoe SB, Sommer AJ, Williams JC Jr, Krambeck AE, Phillips CL, Coe FL. Renal histopathology and crystal deposits in patients with small bowel resection and calcium oxalate stone disease. Kidney Int. 2010a; 78:310–317. [PubMed: 20428098]

Evan AP, Weinman EJ, Wu X-R, Lingeman JE, Worcester EM, Coe FL. Comparison of the pathology of interstitial plaque in human ICSF stone patients to NHERF-1 and THP-null Mice. Urol Res. 2010b; 38:439–452. [PubMed: 21063698]

Fukumoto R, Katayama K, Hayashi T, Matsuoka A, Fujomoto N, Koide T, Kashiwagi H, Tagawa T, Onodera T, Ishida M. Two cases of urolithiiasis induced by topiramate. Hinyokika Kiyo. 2011; 57:125–128. [PubMed: 21586883]

Gambaro G, Favaro S, D'Angelo A. Risk for renal failure in nephrolithiasis. Am J Kidney Dis. 2001; 37:233–243. [PubMed: 11157364]

Gault MH, Chafe LL, Morgan JM, Parfrey PS, Harnett JD, Walsh EA, Prabhakaran VM, Dow D, Colpitts A. Comparison of Patients with Idiopathic Calcium Phosphate and Calcium Oxalate Stones. Medicine. 1991; 70:345–358. [PubMed: 1956278]

Keddis MT, Rule AD. Nephrolithiasis and loss of kidney function. Curr Opin Nephrol Hypertens. 2013; 22:390–396. [PubMed: 23736840]

Kuo RL, Lingeman JE, Evan AP, Parks JH, Bledsoe SB, Patterson RF, Munch LC, Coe FL. Urine calcium and volume predict coverage of renal papilla by Randall's plaque. Kidney Int. 2003; 64:2150–2154. [PubMed: 14633137]

Laerum E, Larsen S. Thiazide prophylaxis of urolithiasis: a double-blind study in general practice. Acta Med Scand. 1984; 215:383–389. [PubMed: 6375276]

Liu YL, Mo L, Goldfarb DS, Evan AP, Liang F, Khan SR, Lieske JC, Wu X-R. Progressive renal papillary calcification and ureteral stone formation in mice deficient for Tamm-Horsfall protein. Am J Physiol. 2010; 299:F469–478.

Miller NL, Gillen DL, Williams JC Jr, Evan AP, Bledsoe SB, Coe FL, Worcester EM, Matlaga BR, Munch LC, Lingeman JE. A formal test of the hypothesis that idiopathic calcium oxalate stones grow on Randall's plaque. BJU Int. 2009; 103:966–971. [PubMed: 19021625]

Pak CYC, Eanes ED, Ruskin B. Spontaneous preciitation of brushite in urine: evidence that brushite is the rius of renal stones originating as calcium phosphate. Pro Natl Acad Sci. 1971; 68:1456–1460.

Pak CYC, Britton F, Peterson R, Ward D, Northcutt C, Breslau NA, McGuire J, Sakhaee K, Bush S, Nicar M, Norman DA, Peters P. Ambulatory evaluation of nephrolithiasis: classification, clinical presentation and diagnostic criteria. Am J Med. 1980; 69:19–30. [PubMed: 6247914]

Parks JH, Worcester EM, Coe FL, Evan AP, Lingeman JE. Clinical implications of abundant calcium phosphate in routinely analyzed kidney stones. Kidney Int. 2004; 66:777–785. [PubMed: 15253733]

Parks JH, Coe FL, Evan AP, Worcester EM. Urine pH in renal calcium stone formers who do and do not increase stone phosphate content with time. Nephrol Dial Transplant. 2009; 24:130–136. [PubMed: 18662977]

Peach RJ, Day WA, Ellingsen PJ, McGiven AR. Ultrastructural localization of Tamm-Horsfall protein in human kidney using immunogold electron microscopy. Histochem J. 1988; 20:156–164. [PubMed: 3410739]

Qiu SR, Ormer CA. Dynamics of biomineral formation at the near-molecular level. Chem Rev. 2008; 108:4784–4822. [PubMed: 19006401]

Tang R, Naacolias GH, Giocondi JL, Hoyer JR, Orme CA. Dual roles of brushite crystals in calcium oxalate crysallization provide physicochemical mechansims underlying renal stone formation. Kidney Int. 2006; 70:71–78. [PubMed: 16641926]

Thurgood LA, Ryall RL. Proteomic analysis of proteins selectively associated with hydroxyapatite, brushite, and uric acid crystals precipitated from human urine. J Proteome Res. 2010; 9:5402–5412. [PubMed: 20795672]

Vervaet BA, Verhulst A, D'Haese PC, De Broe ME. Nephrocalcinosis: new insights into mechanisms and consequences. Nephrol Dial Transplant. 2009; 24:2030–2035. [PubMed: 19297353]

Yasue T. Histochemical identification of calcium oxalate. Acta Histochem Cytochem. 1969; 2:83–95.

Weiss, M.; Liapis, H.; Tomaszewski, JE.; Arend, LJ. Pyelonephriitis and other infections, reflux nephroloathy, hydronephrosis and nephrolithiasis. In: Jennette, JC.; Olson, JL.; Schwarz, MM.; Silva, FG., editors. Heptinstall's pathology of the kidney. Philadelphia, PA: Lippincott Williams and Wilkins; 2007. p. 991-1031.

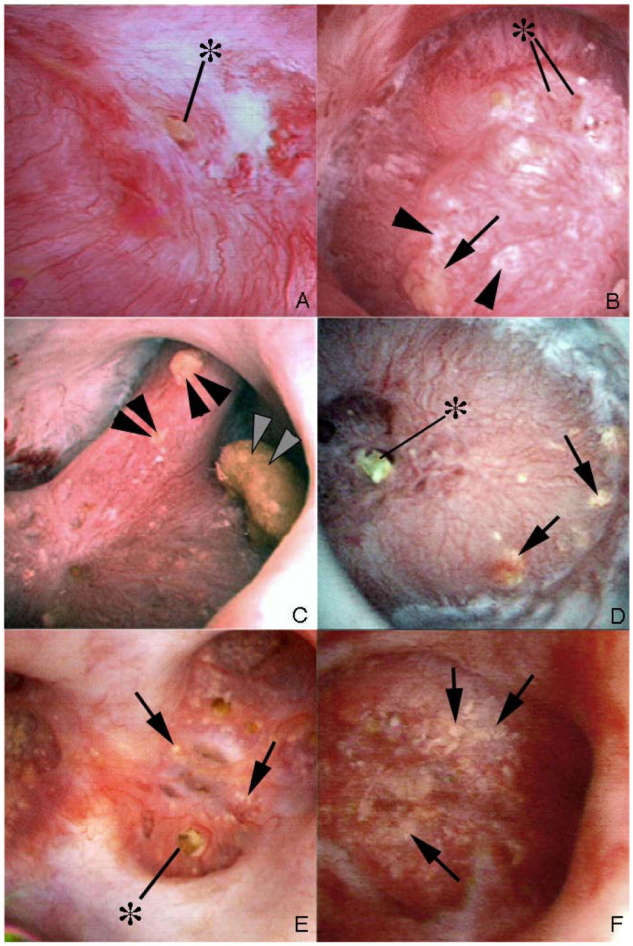

Figure 1. Endoscopic views of renal papilla from HASF

Panel a shows a renal papilla from patient 1 that appears normal except for a protruding plug (asterisk) from a dilated opening of a duct of Bellini. No regions of plaque are noted on the surface of this papilla. In contrast, **panel b** shows a papilla from patient 6 with large sites of Randall's plaque. Several protruding plugs (asterisk) are noted among numerous sites of Randall's plaque (arrowheads) and an occasional site of yellow plaque (arrow). **Panel c** (patient 6) shows three separate attached stones (double arrowheads). The larger stone was determined to be attached to a region of RP and the stone composition was apatite. **Panels d–f** (panel d, patient 7; panel e, patient 5; panel f, patient 3) show the papillary surface of three additional CaP patients that possess regions of yellow plaque (arrows) and little to no Randall's plaque. The two patients 5, 3 (panels e and f) showed papillary retraction and flattening as well as heavy amounts of yellow plaque (arrows). No sites of Randall's plaque were noted in patients 3 and 5.

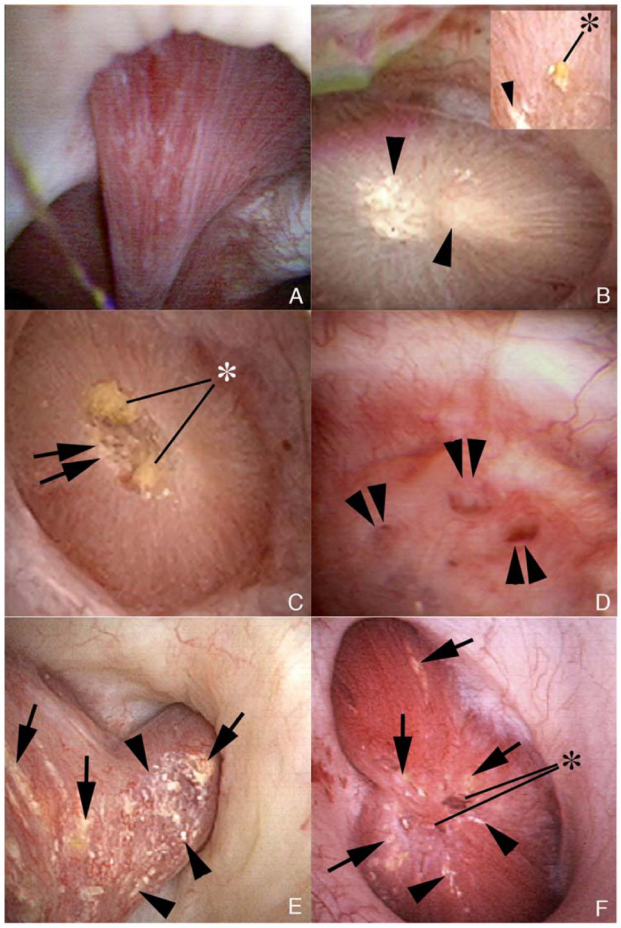

Figure 2. Endoscopic views of renal papilla from new brushite stone formers

Endoscopic mapping of our fifteen new brushite patients showed renal papilla with normal architecture without (panel a, case 25) and with (panels b, e & f; cases 14, 15 & 18 respectively) regions of Randall's plaque. Varying degrees of papillary injury were present which included largely dilated openings of ducts of Bellini with (asterisk, panels c & f; cases 14 & 18) and without (double arrowheads, panel d; case 23) protruding mineral plugs, pitting (double arrows, panel c) and yellow plaque (arrows, panels e & f). Three patients (cases 14, 18, and 22) had CaOx stones attached to sites of Randall's plaque (asterisk, panel b, insert, case 14).

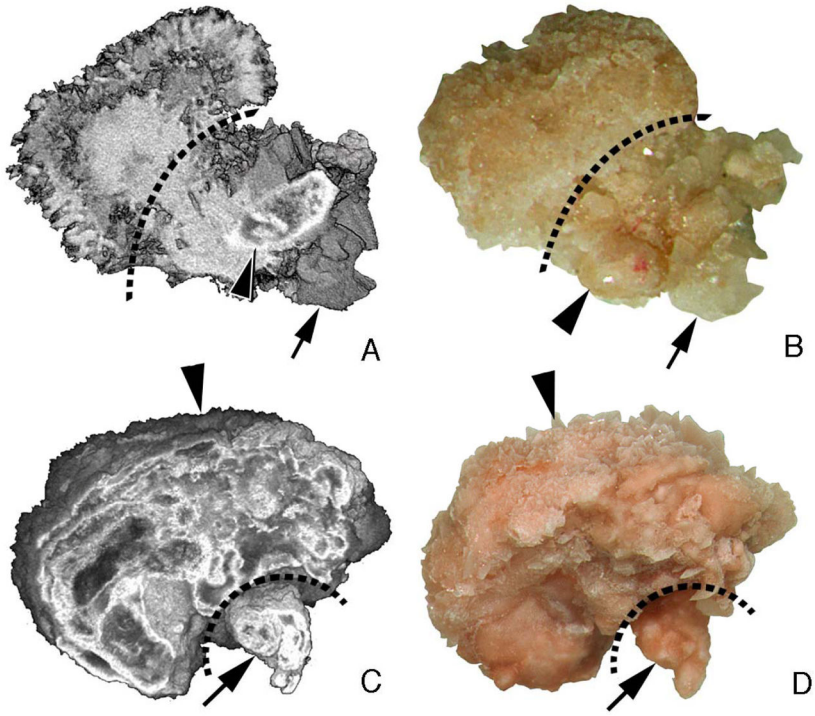

Figure 3. Light microscopic and micro-CT images of stones from a brushite and an apatite patient

Panels a (micro-CT) **and b** (light micrograph) show a stone growing from the distal end of an intralumminal plug protruding from a duct of Bellini in a brushite patient (case 22). A dotted line marks the site of the opening to the duct of Bellini with the stone to the left and the plug to the right. The stone contains primarily brushite and a small surface layer of CaOx while the plug region contains a mixture of apatite (arrowhead), CaOx (arrow) and brushite (rest of the plug). **Panels c** (micro-CT) **and d** (light micrograph) show a stone collected from patient 8. This stone was also attached to the distal end of an intraluminal plug (arrow) that protruded from a dilated opening of a duct of Bellini but in an apatite stone former. Both the stone and plug were multi-layered. The plug portion (arrow) is pure HA while the stone is mostly HA with a trace of calcium oxalate monohydrate located at its surface (arrowhead). Magnification, x20 (a–d).

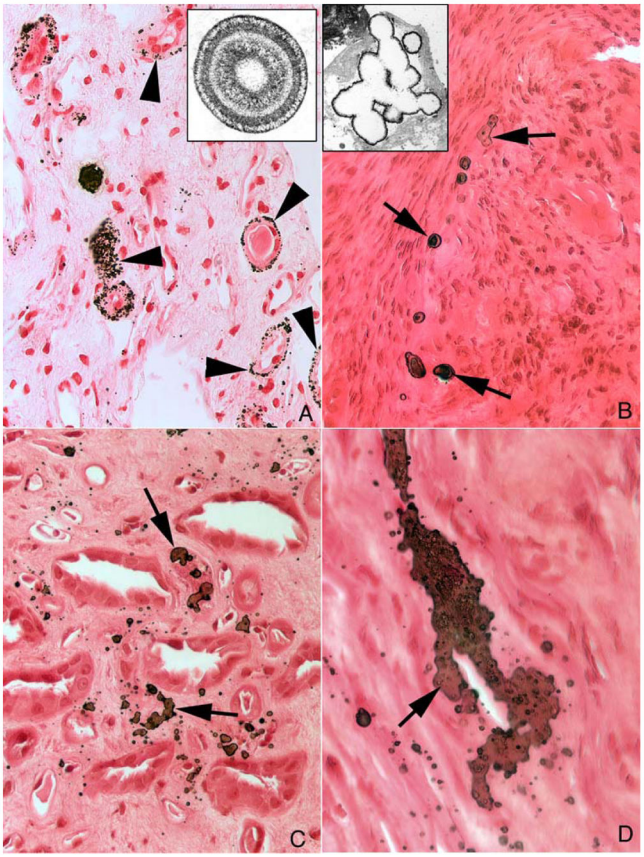

Figure 4. Histologic sections of HA stone formers with sites of sparse to moderate levels of novel interstitial plaque structures (NIPS) compared to sites of Randall's plaque (RP)

RP deposits consist of numerous micro-spherules located primarily in the basement membranes of thin loops of Henle **(arrowheads, panel a; patient 6).** The lamellar structure of RP spherules is detailed in the **insert to panel a. Panel b** shows a region of sparse NIPS deposits (arrows) in patient (case 4) characterized as irregular, large, randomly distributed laminar structures of HA crystal and matrix. The inserts in **panels a and b** contrast the few lamina in NIPS compared to the multiple layers in RP. **Panels c and d** show a patient (case 1) with a moderate amount of NIPS. NIPS deposits (**panel c, arrows)** are irregular in shape, localized to the interstitial space and form large plate-like structures **(panel d, arrow)** surrounding nearby capillaries and thin loops of Henle. Magnification, x1,000 (a–c); x1,500 (d); x35,000 (inserts a and b).

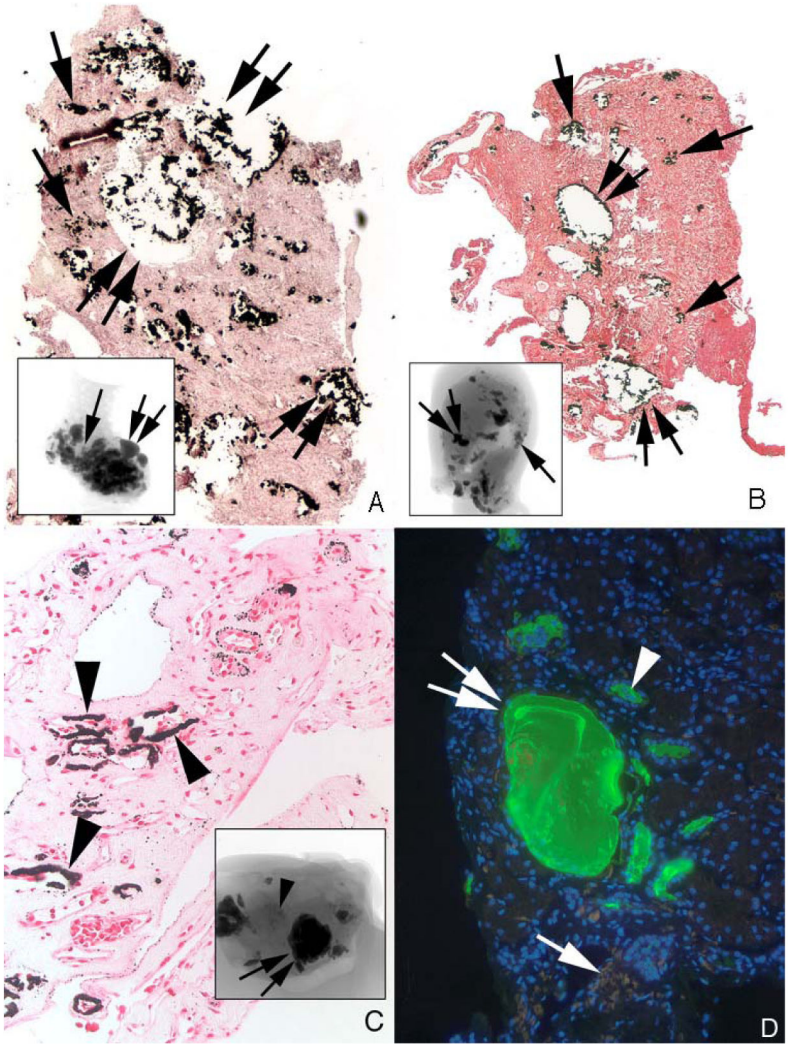

Figure 5. Histologic sections of HA stone formers with sites of large NIPS deposits

Panels a (case 5) **and b** (case 3) show our two HA stone forming patients that possessed large fields of NIPS (single arrows) located near greatly dilated IMCD and BD filled with deposits (double arrows). Extensive regions of interstitial fibrosis surround the dilated collecting ducts and sites of NIPS. **Panel c** shows a site of extensive Randall's plaque (arrowheads) seen in patient 6 but no NIPS. The micro-CT inserts in **panels a and b** show the entire amount of intratubular deposits (double arrows) and regions of NIPS (single arrows) while the insert in **panel c** shows intraluminal deposits (single arrows) and sites of Randall's plaque (arrowhead). In order to determine if sites of NIPS originated as crystal tubular deposits we stained sections containing NIPS with anti-THP antibody **(panel d)**; no staining of sites of NIPS (single arrow) was found even though adjacent normal tubules (arrowhead) and tubules with crystalline deposits (double arrow) stained for THP as expected. Magnification, x500 (a–c), x2,000 (d).

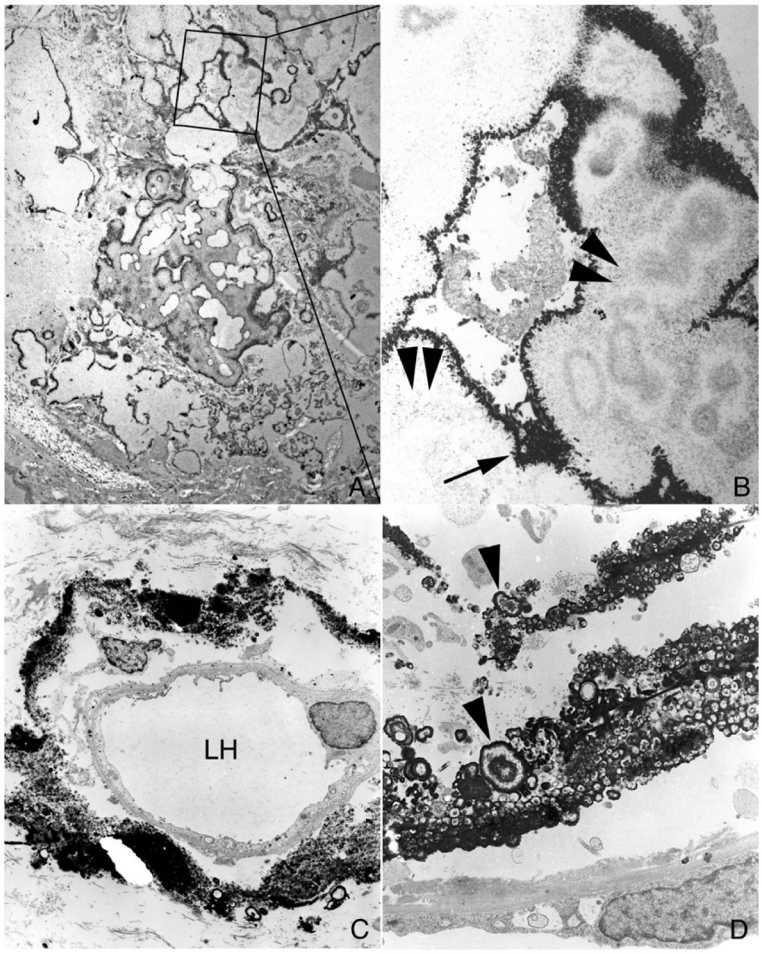

Figure 6. Transmission electron microscopic (TEM) images of large NIPS deposits from patient 5

Panel a shows a low magnification TEM image of a large NIPS deposit that was decalcified prior to sectioning. This extensive deposit is composed of multiple regions of large crystalline material encased in a thin electron dense matrix layer. A selected region of **panel a** (outlined in a box) was enlarged as **panel b** in order to highlight the white crystalline (arrowheads) vs. dark matrix (arrow) areas of the deposit. In contrast, **Panel c** shows a region of Randall's plaque (patient 6) characterized as a crystal island in an organic sea surrounding a loop of Henle (LH). Note the numerous micro-spherules (**Panel d, arrowheads**) surrounded by a dense layer of matrix material. Magnification, x10,000 (a); x20,000(b); x3,000(c); x15,000(d).

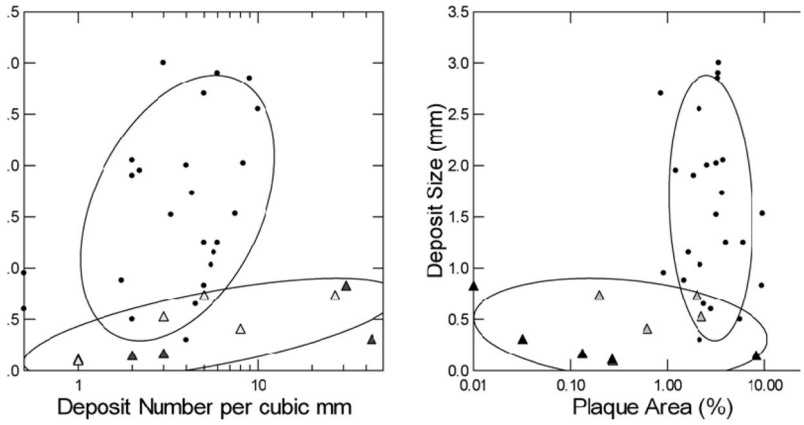

Figure 7. Deposit size, deposit number and white plaque area

Brushite patients (**left panel**, black circles) have deposit sizes ranging from 0.3 to 3 mm, with a majority above 0.5 mm; numbers of deposits/mm^3 range from 1–10. Apatite patients (Triangles) have far smaller deposits at overlapping values for deposit number, and their range of deposit number extends higher than that of brushite patients. Deposit size is unrelated to white plaque area (**right panel**) for both types of patient; plaque area is far smaller among apatite vs. brushite patients. Normal subjects (not shown) have mean plaque areas of 0.5, and no deposits; idiopathic calcium oxalate stone formers also have no deposits but plaque area averages 7.2% of papillary surface. Filled triangles denote presence of NIPS.

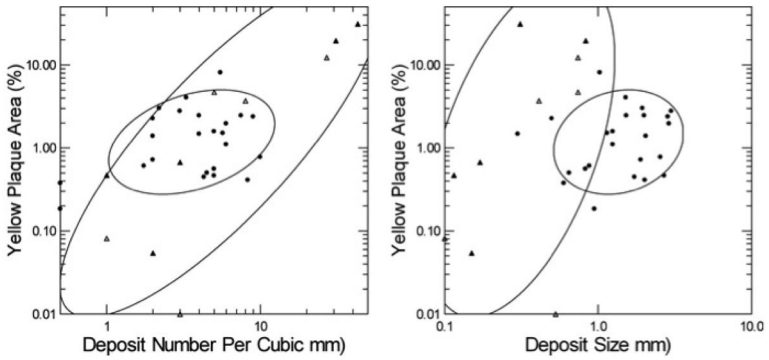

Figure 8. Relationship of yellow plaque to numbers and sizes of intra-tubular deposits

Abundance of yellow plaque (Vertical axes of both panels) varies with numbers of deposits (Left panel) in HASF (triangles) but not BRSF (Circles) and the range of yellow plaque in HASF far exceeds that of BRSF. Yellow plaque does not vary significantly with deposit size (Right panel) in either group. Filled triangles denote patients with NIPS.

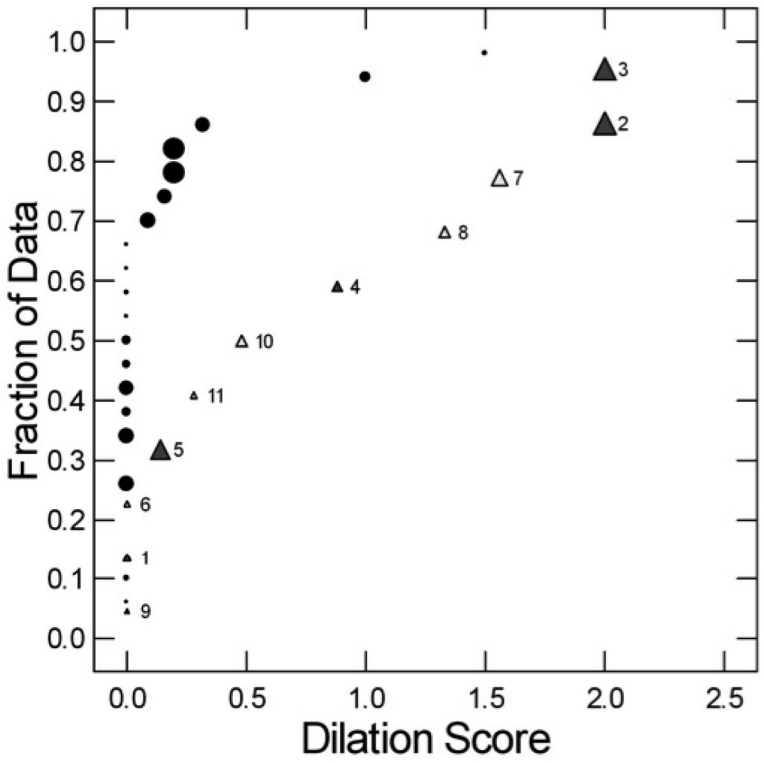

Figure 9. Quantile plot of calyceal dilation and papillary injury in BRSF (black circles) and HASF (Triangles) patients

About 60% of BRSF have no dilation (points aligned along 0 of the x-axis whereas the median dilation for apatite patients is 0.5. Dilation and injury (size of symbols) are not correlated. HASF are identified by their case numbers. **Closed triangles are from patients with NIPS, open without NIPS**.

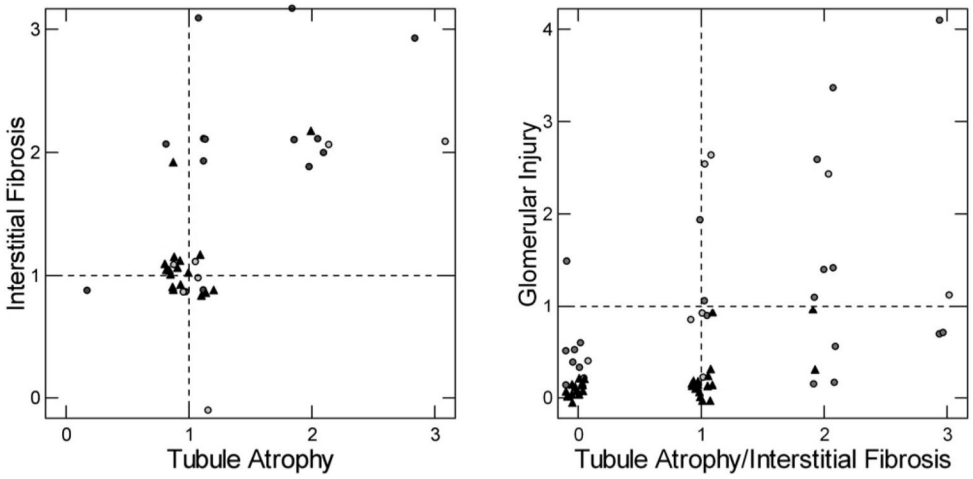

Figure 10. Cortical Interstitial fibrosis and tubular atrophy of brushite (black circles), apatite (open circles) and ICSF (black triangles)

Left panel. A majority of interstitial fibrosis or tubular atrophy scores of 2 or more, denoting significant disease, are in BRSF (statistics in RESULTS). Values <1 are omitted for visual clarity. Points are randomly jittered to permit counting; without this they would overlap at the ordinal intersects. **Right panel**. The highest of interstitial or tubular atrophy score is plotted on the x-axis. On the y axis is plotted the glomerular injury score (METHODS) which sums up the average of mild, moderate and severe changes in sampled glomeruli. The score is calculates so that values above 2 reflect either multiple glomeruli with moderate sclerosis or that glomeruli with mild or absent sclerosis be balanced by some with global sclerosis.

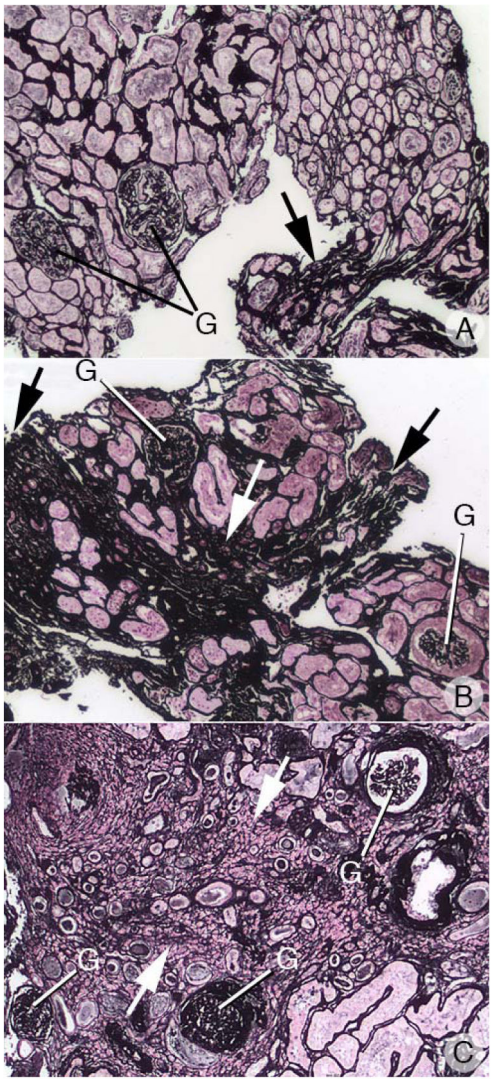

Figure 11. Cortical Interstitial fibrosis, tubular atrophy and glomerulosclerosis in apatite and brushite patients

Panel's a-c shows the range of interstitial (arrows), tubular and glomerular (G) changes seen in the apatite and brushite patients. **Panel a** shows the cortex of an apatite patient with mild interstitial fibrosis and tubular atrophy (score = 1) and no glomerulosclerorsis while **panel b** shows an apatite patient with moderate interstitial fibrosis, tubular atrophy and glomerulosclerorsis (score =2). **Panel c** shows the cortex of a brushite patient with severe interstitial fibrosis, tubular atrophy and glomerulosclerorsis (score =3). Magnification, x1,000(a–c).

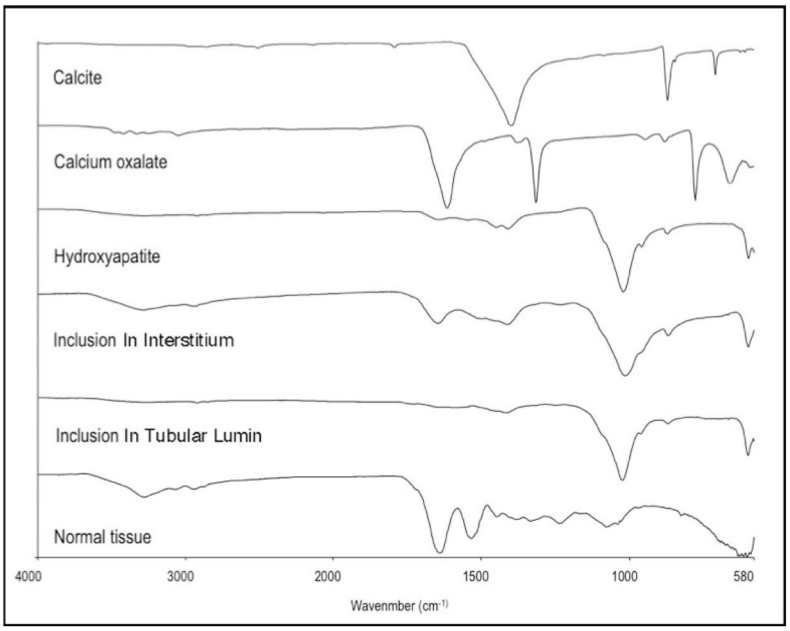

Figure 12. μFTIR analysis of sites of NIPS, Randall's plaque, and intraluminal plugs

This figure illustrates a series of infrared spectra obtained for a set of standards (calcite, calcium oxalate, hydroxyapatite,), for a site of a Yasue-positive papillary, for a site of a Yasue-positive interstitial NIPS deposit from HASF patient 3, intraluminal deposit mineral from HASF patient 5, and for normal tissue with embedding medium. The mineral type in the papillary intraluminal and NIPS deposits were identical to the hydroxyapatite standard. All deposits analyzed from the eleven HASF patients were HA.

TABLE 1

CLINICAL DATA FOR HYDROXYAPATITE AND BRUSHITE STONE FORMERS

Case	Sex	Age 1st stone	Stones	Age at study	ESWL	URS	PNL	UTI	Stone culture	Prior treatment	PMH
1	M	68	2	69	0	0	1	St (−)	St (−)	none	DM, HTN, asthma
2	F	36	2	36	0	0	1	no	NG	none	none
3	F	23	>100	35	0	0	2	EC	NG/NG	K Cit x 10 yr	Crohn's
4	F	35	>30	50	>10	4	3	EC	NG	CTD	EP
5[a]	F	26	>20	37	>5	>5	2	EN, EC, St (−)	CA, EC	none	HTN, PN
6	F	46	>10	56	2	5	1	recurrent	-	none	HTN, AAA, PN
7	F	21	>5	30	1	-	2	EC	-	none	none
8	F	27	1	34	0	0	1	no	NG	none	none
9	M	56	1	56	-	1	1	no	St (−)	none	DM
10	F	23	1	23	-	-	1	EC	St (−), EC	none	PN
11	F	42	13	64	7	8	1	recurrent	NG	Tz, K Cit	none
12	M	13	>13	41	6	3	1	no	-	Tz	None
13	M	26	>13	39	0	5	6	no	-	Tz, NH4Cl	HTN
14	M	26	8	34	>1	0	2	no	NG	none	HTN, THR
15	M	42	>100	63	6	5	3	no	NG	Tz, NH4Cl	HTN, DM, CAD, THR, PE
16	F	16	>200	33	9	5	7	no	NG	Tz, Kcit	HTN, galactorrhea
17	F	15	10	18	1	1	1	no	NG	none	L kidney slow to empty
18	F	34	18	44	0	4	2	no	-	Tz	None
19	F	33	6	37	3	1	3	no	NG	none	None
20	F	48	>5	67	0	0	2	By history	NG	Tz	Hypothyroid
21	F	35	10	39	2	1	1	no	NG	Tz, Kcit	HTN
22	M	42	>12	56	>4	>2	2	no	NG	none	Hypothyroid
23	M	27	>60	46	3	2	1	St (−)	NG	Tz, Kcit	None
24	M	31	7	38	2	0	2	no	NG	Tz	HTN
25	M	28	4	30	2	0	2	no	NG/NG	Kcit	None
26	M	21	>50	34	>4	>4	3	By history	NG	Tz	HTN, urosepsis

[a], nephrocalcinosis, no medullary sponge kidney; ESWL, extracorporeal shock wave lithotripsy; URS, ureteroscopy; PNL, percutaneous nephrolithotomy; UTI, urinary tract infection; PMH, past medical history; St, staph; (−/+), coagulation negative or positive; EC, E Coli; EN, enterococcus; CA, candida albicans; NG, no growth; Tz, thiazide; K Cit, potassium citrate; DM, diabetes mellitus; HTN, hypertension; PN, pyelonephritis; EP, emphysematous PN; AAA, abdominal aortic aneurysm; CAD, coronary artery disease; THR, total hip replacement; PE, pulmonary embolism

TABLE 2

STONE ANALYSES, URINARY TRACT ABNORMALITIES AND CORTICAL INJURY IN STONE FORMERS

Case	Stone Analysis				Initial/Final		GU abnormality	Cortical Injury
	#	Apatite (%)	CaOx (%)	Br (%)	Br (%)	CaOx (%)		
1	1	64	36	-	-	-	Staghorn, ureteritis cystica	None
2	2	40	60	-	-	36/0	Staghorn, bifid ureter, megacalycosis	None
3	3	75	25	-	-	50/13	-	None
4	7	94	6	-	-	0/34	Staghorn, R kidney cortex thinned	Glom
5	5	55	25	20	-	20/4	-	Glom
6	2	82	18	-	-	10/26	-	Glom, Int
7	4[a]	68	32	-	-	-	-	None
8	2[a]	85	15	-	-	-	-	None
9	1	100	-	-	-	-		Int
10	1	74	26	-	-	-	-	-
11	5	60	40	-	-	50/12	-	None
12	7	19	23	57	0/100	-	-	Glom, Int
13	10	0	30	70	0/100	-	-	None
14	2[a]	0	0	100	-	-	-	-
15	5	12	6	82	96/44	-	-	None
16	5	0	0	100	100/100	-	UPJ obstruction	None
17	2	0	33	77	34/100	-	L UPJ obstruction; all stones on L	None
18	3	7	60	33	0/(0/100)[b]	-	R ureteral stricture, dilated ureter	None
19	2[a]	7	46	45	_ [c]	-	Staghorn	None
20	2	0	0	100	100/100	-	Horseshoe kidney	Glom
21	2[a]	0	50	50	_ [d]	-	Staghorn, Persistent R hydro x 2 yr	None
22	3	19	33	48	68/74	-	Staghorn, duplicate collecting system, L hydro	-
23	3	27	10	63	0/100	-	Staghorn, Pyelitis cystica	Int
24	3[a]	20	19	61	_[e]	-	-	None

Case	Stone Analysis				Initial/Final		GU abnormality	Cortical Injury
	#	Apatite (%)	CaOx (%)	Br (%)	Br (%)	CaOx (%)		
25	3	8	48	37	0/(25/85)[f]	-	Long term R staghorn with stents	None
26	6	9	22	69	98/(10/84)	-	-	-

Stone analysis, # of stones analyzed, mineral as % of all stone material analyzed; Initial/final, % BR or HA in first and last stone analyzed;

[a], single stone episode;

[b], L stone 87% CaOx, 13% HA, R stone 100% BR;

[c], L stone 89% CaOx, 11% HA, R stone >90% BR;

[d], L stone 100% COM, R stone 100% Br;

[e], L stones 100% BR, R stone 57% CaOx, 43% HA;

[f], L stones mainly BR, R stones mainly CaOx and HA with thin outer layer BR.

L, left; R, right; UPJ, uretero-pelvic junction; hydro, hydronephrosis; Glom, glomerular injury score ≥ 2; Int, interstitial fibrosis or tubule atrophy score ≥ 2.

TABLE 3

URINE AND SERUM CHEMISTRIES IN HA AND BR STONEFORMERS

Case	Urine volume L/day	Urine pH	Urine calcium mg/day	Urine citrate mg/day	Urine sulfate meq/day	Urine ammonia mmol/day	Urine Ox mg/day	SS CaOx	SS CaP	Serum creat mg/dl	Serum HCO_3 mmolL	Serum calcium mg/dl
Normal range	> 1.5	5.8–6.2	100–200	500–750	20–80	15–50	30–55			0.8–1.2	24–29	9–10
1	2.82	6.38	489	840	69	19	36	5.4	2.15	1.3	31	9.3
2	2.11	6.58	226	648	19	20	24	4.9	1.44	0.6	29	9.6
3	1.63	6.18	289	241	50	24	23	5.5	1.84	0.8	24	9.4
4	1.10	5.95	115	344	28	26	36	8.3	0.76	0.9	27	9.3
5	1.78	6.32	325	518	36	15	41	11	1.9	0.9	25	9.8
6	1.35	5.94	378	265	30	29	30	11	2.6	0.5	25	8.2
7	-	-	-	-	-	-	-	-	-	0.7	24	8.4
8	1.52	6.43	220	299	35	28	22	6.7	2.35	0.8	28	9.9
9	1.53	5.62	253	826	44	23	47	11	0.23	0.9	30	9.2
10	-	-	-	-	-	-	-	-	-	0.8	-	-
11	1.11	5.84	242	133	23	23	26	12.6	1.69	0.8	29	9.7
12	1.25	6.38	395	804	29	17	37	13.5	3.2	1.4	28	9.7
13	2.27	6.06	580	1282	70	23	53	12.3	2.7	1.7	26	10.8
14	-	-	-	-	-	-	-	-	-	1.4	30	8.9
15	2.60	6.30	493	802	73	-	53	9.46	2.0	1.1	25	9.4
16	1.84	6.23	180	37	34	42	30	5.24	1.2	1.0	24	9.9
17	1.94	6.73	193	301	25	12	33	6.10	2.0	0.95	24	7.9
18	1.58	6.25	290	447	32	28	29	8.99	2.2	0.9	25	9.6
19	2.71	6.25	454	1215	37	52	40	8.74	2.5	0.8	23	9.3
20	1.90	6.25	269	160	20	16	23	5.20	2	1.0	28	9.2
21	1.68	6.40	255	184	16	18	26	6.53	1.9	0.9	24	9.5
22	3.19	6.69	253	672	33	15	53	5.55	0.9	1.1	27	10.1
23	1.94	6.38	372	698	61	35	42	8.55	3.3	0.8	24	9.5
24	3.40	6.64	140	219	66	70	41	2.54	0.7	1.2	28	10.1

Case	Urine volume L/day	Urine pH	Urine calcium mg/day	Urine citrate mg/day	Urine sulfate meq/day	Urine ammonia mmol/day	Urine Ox mg/day	SS CaOx	SS CaP	Serum creat mg/dl	Serum HCO_3 mmolL	Serum calcium mg/dl
25	-	-	-	-	-	-	-	-	-	1.4	26	10.2
26	2.38	6.34	477	997	86	72	68	11.6	2.8	0.8	28	9.1

Table 4

This Table Summarizes Differences Between Three Stone Phenotypes.

	ICSF	BRSF	HASF
pH	6 ±0.01	6.3 ±0.05*	6.3 ±0.04*
SS CaP	1.54 ±0.04	2.3 ±0.1*	2 ±0.1*
SS CaOx	9.7 ±0.2	10.1 ±0.6	9 ±0.5
Ca mg/d	237 ±3	297 ±12*	271 ±10*
RP % SURFACE	8	6	0.8
DEPOSITS/MM^3	0	**4**	**12**
DEPOSIT MM^2	0	1.6	0.4
STONES ON RP	**10/patient**	**3/25 patients**	**6/11 patients**
DILATION	0.2	0.17	0.8
INJURY	0.18	0.37	0.58
TIF OR G >1	2/30 6.7%	13/21 62%	4/11 36.4%
BR IN STONES	**0**	**>0**	**0**

SS CaP, calcium phosphate supersaturation; SS CaOx, calcium oxalate supersaturation; Ca mg/d, urinary calcium in milligrams per day. RP, Randall's plaque; TIF, tubule-interstitial fibrosis, G, glomerular; BR, brushite.